Flutter Analysis of Annular Cascades in Counter Rotation

R. Nishino and M. Namba
Sojo University
Ikeda, Kumamoto, 860-0082, Japan
E-mail *namba@arsp.sojo-u.ac.jp*

Keywords: Flutter, Cascade, Multiple Blade Rows, Unsteady Aerodynamics, Aeroelasticity

Abstract

The paper studies the effect of neighboring blade rows on flutter characteristics of cascading blades. For this purpose the computation program to calculate the unsteady blade loading based on the unsteady lifting surface theory for contra-rotating annular cascades was formulated and coded. Then a computation program to solve the coupled bending-torsion flutter equation for the contra-rotating annular cascades was also developed. Some results of the flutter analysis are presented. The presence of the neighboring blade row gives rise to significant change in the critical flutter condition when the main acoustic duct mode is of cut-on state.

Introduction

The unsteady aerodynamic force on oscillating blades in a cascade is heavily dependent on the interblade phase angle. This implies that the aerodynamic coupling among blades plays a critical role on the cascade flutter characteristics. From this standpoint neighboring blade rows, e.g., a neighboring rotor or stator or contra-rotating fan cascade, also will have a considerable influence on the unsteady aerodynamic force because blade rows are closely placed in actual turbomachines.

There are available a few published papers dealing with the influence of neighboring blade rows on the unsteady aerodynamic response of oscillating blades. The theoretical study based on the semi-actuator disk model by Tanida[1] and the experiments and the linear cascade theory by Kobayashi et al[2, 3] should be cited as the earliest works. Their works show only a minor importance of the multistage coupling for the cascade flutter. Their theories, however, assume incompressible flows and therefore can not deal with aeroacoustic interaction between blade rows via cut-on acoustic duct modes.

Since then until recently no paper dealing with the subject was published except a Russian paper by Butenko and Osipov[4], which developed a theory for subsonic linear cascades in relative motion.

The extension of the study of the cascade flutter to multistage cascades is recently drawing the interest of turbomachinery aerodynamicists. Hall and Silkowski[5] presented an analysis based on two-dimensional subsonic multiple blade rows, and Namba et al.[7] developed a three-dimensional theory for oscillating subsonic contra-rotating annular cascades. Those studies for subsonic flows indicate that the influence of aeroacoustic coupling among blade rows on the aerodynamic damping force is significant in particular when the main acoustic duct mode generated from the oscillating blade row is cut-on. It suggests that in the case of supersonic cascades, where oscillation of blades generates an infinite number of cut-on modes, neighboring blade rows will be much more influential.

The author[8] extended his study to supersonic contra-rotating annular cascades, where relative mean fluid velocities for both cascades are supersonic, and gave numerical results showing a crucial difference in unsteady aerodynamic work on oscillating blades between aerodynamically decoupled and coupled cascades. However some bugs which result in exaggeration of the difference were later found in the computation codes.

The program has been improved and further extended[11] so that it can deal with the combination of supersonic and subsonic cascades, for instance, a supersonic rotor cascade and a subsonic stator cascade. Hall et al.[6] developed a three-dimensional Euler solver for computing unsteady flows in vibrating multistage cascades. In their paper comparison is made of a model problem between the computations by their Euler solver and the author's lifting surface theory, and an excellent agreement is demonstrated.

The present computation program based on the unsteady lifting surface theory[9, 10] is able to provide aerodynamic forces on oscillating blades as functions of the frequency. The computation speed is remarkably high, so that it can be a very efficient tool to calculate aerodynamic force terms of the flutter equations.

A computation program to solve the coupled bending-torsion flutter equation for the contra-rotating annular cascades was formulated and coded, and an application to the flutter analysys was briefly mentioned in the previous paper[11] .

This paper presents further details of the method of flutter analysis, and some numerical results demonstrating the significant influence of the neighboring blade row on the cascade flutter boundaries.

Outline of the Analytical Method

Model Description

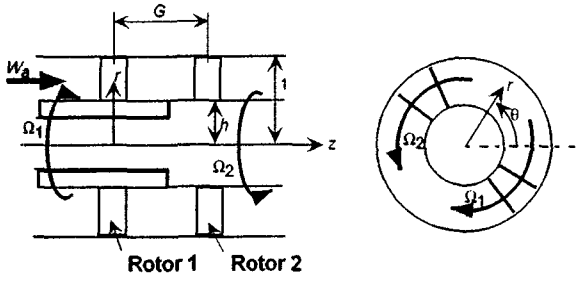

Figure 1: Contra-rotating annular cascades.

We consider a pair of annular cascades in an annular duct of infinite axial extent with the outer duct radius r_T^* and the boss ratio h as shown in Figure 1. The undisturbed flow is a uniform axial flow of axial velocity W_a^*, static pressure p_0^* and fluid density ρ_0^*. In the following unstarred symbols denote dimensionless quantities, where lengths, velocities, pressures and times are scaled with respect to r_T^*, W_a^*, $\rho_0^* W_a^{*2}$ and r_T^*/W_a^*, respectively. Let subscripts 1 and 2 denote the upstream rotor 1 and the downstream rotor 2. Further following notations are used: N_{B1} and N_{B2}: numbers of blades, $\Omega_1 = \Omega_1^* r_T^*/W_a^* (\geq 0$, clockwise looking from a downstream station) and $\Omega_2 (\leq 0$, anti-clockwise): rotational angular velocities of the rotors, C_{a1} and C_{a2}: axial chord length assumed constant along the span, (r, θ, z), (r, θ_1, z_1) and (r, θ_2, z_2): cylindrical coordinates in the frames fixed to the duct, rotor 1 and rotor 2 respectively. The angle coordinates and axial coordinates of different frames are related to each other by

$$\theta = \theta_1 - \Omega_1 t = \theta_2 - \Omega_2 t, \quad z = z_1 = z_2 + G. \quad (1)$$

Here t denotes the time coordinate and G denotes the axial distance between the centers of rotor 1 and rotor 2.

We assume that the steady blade loading is zero, i.e., the time mean flow is uniform, and that the unsteady disturbances induced by blade vibrations are small. Therefore the unsteady flow is governed by linearized equations.

Multiplication of Blade Loading Frequency

Assume that the blades of rotor 1 are vibrating with a single frequency ω $(= \omega^* r_T^*/W_a^*)$ and an inter-blade phase angle $2\pi\sigma/N_{B1}$, so that the displacement normal to the blade chord of the m-th blade is given by

$$a_1(r, z) e^{i\omega t + i2\pi\sigma m/N_{B1}} : \ m = 0, 1, ..., N_{B1} - 1. \quad (2)$$

Here σ is an integer between $-N_{B1}/2$ and $N_{B1}/2$.

Then as described in details in references [7, 8], aeroacoustic coupling between the rotors in mutual motion produces flow disturbances of multiple frequencies, resulting in blade loading of multiple frequencies. Thus we can describe the unsteady blade loading (pressure difference between upper and lower surfaces of blades) on the m-th blade of each rotor as summations of multiple frequency components:

$$\sum_{\nu=-\infty}^{\infty} \Delta p_{1-1,(\nu)}(r, z_1) e^{i\omega_{1\nu} t + i2\pi\sigma_{1\nu} m/N_{B1}} \quad (3)$$

and

$$\sum_{\mu=-\infty}^{\infty} \Delta p_{2-1,(\mu)}(r, z_2) e^{i\omega_{2\mu} t + i2\pi\sigma_{2\mu} m/N_{B2}}, \quad (4)$$

where

$$\omega_{1\nu} = \omega - \nu N_{B2}(\Omega_1 - \Omega_2), \quad (5)$$
$$\sigma_{1\nu} = \nu N_{B2} + \sigma, \quad (6)$$
$$\omega_{2\mu} = \omega + (\mu N_{B1} + \sigma)(\Omega_1 - \Omega_2), \quad (7)$$
$$\sigma_{2\mu} = \mu N_{B1} + \sigma. \quad (8)$$

Further subscripts 1-1 and 2-1 imply the loading on rotor 1 blades due to vibration of rotor 1 blades themselves and the loading on rotor 2 blades due to vibration of rotor 1 blades respectively. It is worth emphasizing that all frequency components are coupled with each other and can not be determined independently.

In the case of blade vibration of rotor 2 with displacement normal to blade surface given by

$$a_2(r, z_2) e^{i\omega t + i2\pi\sigma m/N_{B2}} : \ m = 0, 1, ..., N_{B2} - 1, \quad (9)$$

similar formulations can be made, and the blade loadings may be written as

$$\sum_{\nu=-\infty}^{\infty} \Delta p_{2-2,(\nu)}(r, z_2) e^{i\omega_{2\nu} t + i2\pi\sigma_{2\nu} m/N_{B2}} \quad (10)$$

and

$$\sum_{\mu=-\infty}^{\infty} \Delta p_{1-2,(\mu)}(r, z_1) e^{i\omega_{1\mu} t + i2\pi\sigma_{1\mu} m/N_{B1}}, \quad (11)$$

where

$$\omega_{2\nu} = \omega - \nu N_{B1}(\Omega_2 - \Omega_1), \quad (12)$$
$$\sigma_{2\nu} = \nu N_{B1} + \sigma, \quad (13)$$
$$\omega_{1\mu} = \omega + (\mu N_{B2} + \sigma)(\Omega_2 - \Omega_1), \quad (14)$$
$$\sigma_{1\mu} = \mu N_{B2} + \sigma. \quad (15)$$

Acoustic Modes and Frequencies

In the present problem disturbances are composed of multiple frequencies and multiple acoustic duct modes. The frequencies $\omega_{\nu,\mu}$ viewed in the frame fixed to the duct, i.e., (r, θ, z) system, and corresponding circumferential wave numbers $n_{\mu,\nu}$ of the

Table 1: Frequencies and circumferential wave numbers of duct modes.

Case	Frequency $\omega_{\mu,\nu}$	Wave number $n_{\mu,\nu}$
Vibration of rotor 1	$\omega + \mu N_{B1}\Omega_1 + \nu N_{B2}\Omega_2 + \sigma\Omega_1$	$\mu N_{B1} + \nu N_{B2} + \sigma$
Vibration of rotor 2	$\omega + \mu N_{B2}\Omega_2 + \nu N_{B1}\Omega_1 + \sigma\Omega_2$	$\mu N_{B2} + \nu N_{B1} + \sigma$

duct modes are given in Table 1. Hereafter we denote the acoustic duct mode of $(n_{\mu,\nu}, \ell)$ by $(\mu, \nu;\ \ell)$, where ℓ denotes the radial order. A mode $(\mu, \nu;\ \ell)$ is cut-off if

$$\left(k_\ell^{(n_{\mu,\nu})}\right)^2 - \omega_{\mu,\nu}^2 M_a^2/(1 - M_a^2) > 0, \qquad (16)$$

where $k_\ell^{(n)}$ denotes the radial eigenvalue[9, 10], and M_a is the axial Mach number. Solving the inequality (16) for the blade vibration frequency ω, we can write

$$\omega^-_{\mu,\nu,\ell}(\sigma) < \omega < \omega^+_{\mu,\nu,\ell}(\sigma), \qquad (17)$$

where the critical cut-off frequencies are given by

$$\omega^\pm_{\mu,\nu,\ell}(\sigma) = \pm\sqrt{\frac{1 - M_a^2}{M_a^2}\left(k_\ell^{(n_{\mu,\nu})}\right)^2} - (\mu N_{B1}\Omega_1 + \nu N_{B2}\Omega_2 + \sigma\Omega_1), \qquad (18)$$

in the case of vibration of rotor 1 blades. Note that the expression for the case of vibration of rotor 2 blades can simply be obtained by exchanging the subscript 1 for 2 and 2 for 1.

Under this notation of the duct modes we can state that vibrating blades directly generate $(\mu, 0;\ \ell)$ modes. Hereafter let us call the modes of $\nu = 0$ the primary duct modes, and the modes of $\nu \neq 0$ the secondary duct modes.

If all of the primary duct modes are cut-off and if the rotors are remotely separated, the influence of the neighboring blade row will not be substantial. We should note, however, that vortical disturbances are convected without decaying. Therefore in the case of vibration of rotor 1, the vortical disturbances from rotor 1 always exert a finite influence on rotor 2 even if all primary duct modes $(\mu, 0;\ \ell)$ are cut-off and however large the rotor-to-rotor distance G may be. Further, any of the secondary duct modes of $\nu \neq 0$ resulting from the interaction can be cut-on, giving backward reaction to rotor 1. The previous studies[7] indicate, however, that the vortical disturbances play only a minor role in the aerodynamic interaction between the blade rows.

Note that $\Omega_1\Omega_2 < 0$ in the case of contra-rotating cascades. Therefore duct modes of $\mu\nu < 0$ are of high frequency and low circumferential wave number, and are likely to satisfy the cut-on condition.

Determination of Aerodynamic Force

The lifting surface theory represents the disturbance flow field as summation of disturbances induced by unsteady blade loadings of both rotors. The disturbance flow quantities are mathematically expressed in integral forms involving blade loading functions $\Delta p_{1-1,(\nu)}(r, z)$, etc. Once the blade loading functions are determined, the disturbance flow quantities are obtained by straightforward computation of the integrals.

In the present problem the blade loading functions are not prescribed but are unknown functions to be determined. The flow tangency condition at the blade surfaces gives a set of simultaneous integral equations for the unsteady blade loading functions $\Delta p_{1-1,(\nu)}(r, z)$: $\nu = 0, \pm1, \pm2, ...$ and $\Delta p_{2-1,(\mu)}(r, z)$: $\mu = 0, \pm1, \pm2, ...$ (the case of rotor 1 vibration), or $\Delta p_{1-2,(\mu)}(r, z)$: $\mu = 0, \pm1, \pm2, ...$ and $\Delta p_{2-2,(\nu)}(r, z)$: $\nu = 0, \pm1, \pm2, ...$ (the case of rotor 2 vibration) as shown in Appendix I. There are available various methods to solve the equations numerically. A method based on combination of Galerkin formulation and expansion of blade loading functions in terms of double mode function series is applied to the present study. Details are omitted to save space.

Coupled Bending-Torsion Vibration of Blades

Consider the blades of either of the rotors are oscillating at an frequency ω and an interblade phase angle $2\pi\sigma/N_B$. Hereafter the suffix 1 or 2 denoting the rotor number is omitted. As shown in Fig. 2 we describe the displacement of a blade normal to the blade surface by

$$a(r, s, t) = \eta(r, t) + \{s - s_e(r)\}\phi(r, t), \qquad (19)$$

where $\eta(r, t)$ denotes the bending displacement normal to local blade chord and $\phi(r, t)$ denotes the torsional displacement about an elastic axis $s = s_e(r)$ $(z = z_e(r))$. Here s denotes a local chordwise coordinate i.e., $ds = \sqrt{1 + \Omega^2 r^2}dz$. Further express the bending and torsional displacements by

$$\eta(r, t) = \sum_{j=1}^{\infty} Z_j(r)\eta_j e^{i\omega t}, \qquad (20)$$

$$\phi(r, t) = \sum_{j=1}^{\infty} \Phi_j(r)\phi_j e^{i\omega t}, \qquad (21)$$

where $Z_j(r)$ and $\Phi_j(r)$ denote normalized j-th bending and j-th torsional natural mode shape functions respectively, and η_j and ϕ_j denote the modal amplitudes, which are complex numbers. The natural modes imply the vibration modes in vacuum.

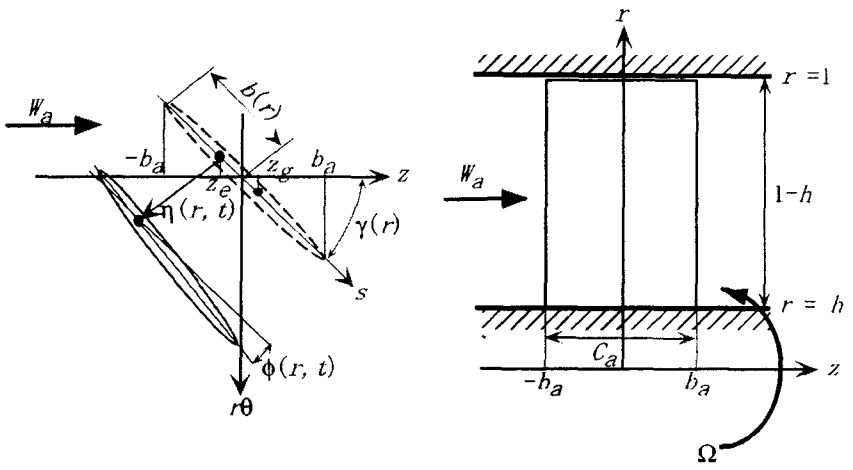

Figure 2: An oscillating blade in a rotating annular cascade.

As described by equations (3) and (10), the aerodynamic force on vibrating blades under the aerodynamic interaction between the two blade rows is of multiple frequencies, but one should note that the blade motion of the frequency ω can only be excited or damped by the fundamental frequency component ($\nu = 0$) of the aerodynamic force.

Therefore let the fundamental frequency component of the blade surface pressure difference due to the blade motion described by equations (19)-(21) be expressed by

$$\Delta p(r,s,t) = \sum_{j=1}^{\infty} \Delta p_{Bj}(r,s)\eta_j e^{i\omega t}/b_a + \sum_{j=1}^{\infty} \Delta p_{Tj}(r,s)\phi_j e^{i\omega t}. \quad (22)$$

Here $\Delta p_{Bj}(r,s)\eta_j e^{i\omega t}/b_a$ and $\Delta p_{Tj}(r,s)\phi_j e^{i\omega t}$ denote the unsteady lifting pressure due to j-th mode bending motion ($Z_j(r)\eta_j e^{i\omega t}$) and the unsteady lifting pressure due to j-th mode torsional motion about $s = s_e(r)$ ($\Phi_j(r)\phi_j e^{i\omega t}$) respectively. Here $b_a = C_a/2$ denotes the semi-axial-chord.

Note again that blades are aerodynamically coupled although they are mechanically decoupled. Therefore the lifting pressure includes the effect of the aerodynamic coupling among all blades of both blade rows.

Neglecting the mechanical damping, we can describe the equation of the blade motion as a balance of the inertia, stiffness and aerodynamic forces as follows:

$$-\lambda^2(\boldsymbol{M}+\boldsymbol{S})\boldsymbol{y} + \boldsymbol{K}\boldsymbol{y} = \boldsymbol{A}\boldsymbol{y}, \quad (23)$$

where λ is the reduced frequency defined by

$$\lambda = \omega b_a = \omega^* b_a^*/W_a^*. \quad (24)$$

Here $\boldsymbol{y}$ denotes the blade displacement, which is a column vector:

$$\boldsymbol{y} = \begin{Bmatrix} \boldsymbol{y}_1 \\ \boldsymbol{y}_2 \\ \vdots \end{Bmatrix}, \quad \boldsymbol{y}_k = \begin{Bmatrix} \eta_k/b_a \\ \phi_k \end{Bmatrix}. \quad (25)$$

On the other hand, $\boldsymbol{M}$, $\boldsymbol{S}$, $\boldsymbol{K}$ and $\boldsymbol{A}$ are mass, static mass moment, stiffness and aerodynamic force matrices, the $\boldsymbol{kj}$-th elements of which are given by the following 2×2 submatrices:

$$\boldsymbol{M}_{kj} = \mu_{ba}\begin{bmatrix} M_k & 0 \\ 0 & r_e^2\bar{I}_k \end{bmatrix}\delta_{kj}, \quad (26)$$

$$\boldsymbol{S}_{kj} = \mu_{ba}x_{eg}\begin{bmatrix} 0 & \bar{S}_{kj} \\ \bar{S}_{jk} & 0 \end{bmatrix}, \quad (27)$$

$$\boldsymbol{K}_{kj} = \mu_{ba}\begin{bmatrix} M_k\lambda_{Bk}^2 & 0 \\ 0 & r_e^2\bar{I}_k\lambda_{Tk}^2 \end{bmatrix}\delta_{kj}, \quad (28)$$

$$\boldsymbol{A}_{kj} = \begin{bmatrix} L_{Bkj} & L_{Tkj} \\ M_{Bkj} & M_{Tkj} \end{bmatrix}. \quad (29)$$

Here δ_{kj} denotes the Kronecker delta. Further

$$\lambda_{Bk} = \omega_{Bk}^* b_a^*/W_a^*, \quad \lambda_{Tk} = \omega_{Tk}^* b_a^*/W_a^*, \quad (30)$$

denote dimensionless bending and torsional natural mode frequencies of order k. The definitions of the mass ratio μ_{ba}, the averaged dimensionless radius of gyration r_e, the averaged dimensionless distance between the center of gravity and the elastic axis x_{eg}, the dimensionless generalized modal mass $\bar{M}_k$, modal moment of inertia $\bar{I}_k$ and modal static mass moment $\bar{S}_{kj}$, and the dimensionless generalized modal aerodynamic forces, L_{Bkj}, L_{Tkj}, M_{Bkj} and M_{Tkj}, are given in Appendix II.

Determination of Flutter Condition

After some algebraic manipulations equation (23) can be rewritten into

$$[\boldsymbol{C} - X\boldsymbol{I}]\boldsymbol{y} = 0. \quad (31)$$

Here I is unit matrix, and X is defined by

$$X = \frac{\lambda_{B1}^2}{\lambda^2} = \frac{\omega_{B1}^{*2}}{\omega^{*2}}, \tag{32}$$

Further C is a complex matrix, the kj-th element of which is given by a submatrix:

$$C_{kj} = \begin{bmatrix} \frac{1}{\bar{\omega}_{Bk}^2}\delta_{kj} & \frac{1}{\bar{\omega}_{Bk}^2 M_k} x_{eg} \bar{S}_{kj} \\ \frac{1}{\bar{\omega}_{Tk}^2 r_e^2 \bar{I}_k} x_{eg} \bar{S}_{jk} & \frac{1}{\bar{\omega}_{Tk}^2}\delta_{kj} \end{bmatrix} + \frac{1}{\mu_{ba}\lambda^2} \begin{bmatrix} \frac{L_{Bkj}}{\bar{\omega}_{Bk}^2 \bar{M}_k} & \frac{L_{Tkj}}{\bar{\omega}_{Bk}^2 \bar{M}_k} \\ \frac{M_{Bkj}}{\bar{\omega}_{Tk}^2 r_e^2 \bar{I}_k} & \frac{M_{Tkj}}{\bar{\omega}_{Tk}^2 r_e^2 \bar{I}_k} \end{bmatrix}, \tag{33}$$

where

$$\bar{\omega}_{Bk} = \lambda_{Bk}/\lambda_{B1} = \omega_{Bk}^*/\omega_{B1}^*, \tag{34}$$

$$\bar{\omega}_{Tk} = \lambda_{Tk}/\lambda_{B1} = \omega_{Tk}^*/\omega_{B1}^*. \tag{35}$$

Then X and $\boldsymbol{y}$ can be determined as eigenvalues and eigenvectors of the matrix $\boldsymbol{C}$ respectively. Let the eigenvalues and eigenvectors be denoted by

$$X^{(m)} : \ m = 1, 2, \ldots, \tag{36}$$

$$\boldsymbol{Y} = \left[\boldsymbol{y}^{(1)}, \boldsymbol{y}^{(2)}, \ldots\right] \tag{37}$$

$$= \begin{bmatrix} \boldsymbol{y}_1^{(1)} & \boldsymbol{y}_1^{(2)} & \cdots \\ \boldsymbol{y}_2^{(1)} & \boldsymbol{y}_2^{(2)} & \cdots \\ \boldsymbol{y}_3^{(1)} & \boldsymbol{y}_3^{(2)} & \cdots \\ \vdots & \vdots & \ddots \end{bmatrix}, \tag{38}$$

where

$$\boldsymbol{y}_k^{(m)} = \begin{Bmatrix} \eta_k^{(m)}/b_a \\ \phi_k^{(m)} \end{Bmatrix} : \ k = 1, 2, \ldots; \ m = 1, 2, \ldots.$$

Now note that the matrix $\boldsymbol{C}$ is governed by elastic and structural parameters: μ_{ba}, x_{eg}, r_e^2, $\bar{M}_k$, $\bar{I}_k$, $\bar{S}_{kj}$, $\bar{\omega}_{Bk}$, $\bar{\omega}_{Tk}$, and parameters of blade row configuration on which the aerodynamic force terms are dependent: Ω_1, Ω_2 (rotational speeds), N_{B1}, N_{B2} (numbers of blades), C_{a1}, C_{a2} (axial chord lengths), h (boss ratio), G (distance between the blade row centers), M_a (axial Mach number), λ (reduced frequency), σ (interblade phase parameter) and the blade profile shapes.

Let all elastic and aerodynamic parameters other than λ be specified. Then the eigenvalues $X^{(m)}$ and the eigenvectors $\boldsymbol{Y}$ are functions of the reduced frequency λ. Put

$$\frac{1}{\sqrt{X^{(m)}(\lambda)}} = f^{(m)}(\lambda) + i\, g^{(m)}(\lambda). \tag{39}$$

Then the m-th mode flutter occurs at the reduced frequency $\lambda = \lambda_F^{(m)}$ that satisfies

$$g^{(m)}(\lambda_F^{(m)}) = 0. \tag{40}$$

The expressions for the m-th mode flutter velocity and flutter frequency are given by

$$W_{aF}^{(m)} = b_a \omega_{B1} \frac{f^{(m)}(\lambda_F^{(m)})}{\lambda_F^{(m)}}, \tag{41}$$

$$\omega_F^{(m)} = \omega_{B1} f^{(m)}(\lambda_F^{(m)}). \tag{42}$$

The blade motion at the m-th mode flutter is given by

$$a(r, s, t)^{(m)} \propto e^{i\omega_F^{(m)} t} \left[\sum_{k=1}^{\infty} Z_k(r)\eta_k^{(m)} + \sum_{k=1}^{\infty}(s - s_e(r))\Phi_k(r)\phi_k^{(m)}\right] \tag{43}$$

where

$$\begin{Bmatrix} \eta_k^{(m)}/b_a \\ \phi_k^{(m)} \end{Bmatrix} = \boldsymbol{y}_k^{(m)}(\lambda_F^{(m)}). \tag{44}$$

The most probable flutter mode will be that corresponding to the lowest flutter velocity. Hence

$$W_{aF} = b_a \omega_{B1} \min\left(\frac{f^{(1)}(\lambda_F^{(1)})}{\lambda_F^{(1)}}, \frac{f^{(2)}(\lambda_F^{(2)})}{\lambda_F^{(2)}}, \ldots\right), \tag{45}$$

Note that to search the condition (40) we should compute the aerodynamic force terms for various values of λ. To this end computation by CFD may be too time-consuming. On the other hand the present analytical method is a very useful aerodynamic tool, which can provide numerical values of aerodynamic force terms for a given reduced frequency within a few seconds on a modern personal computer.

Numerical Results and Discussion

Conditions Investigated

The results presented in this paper are restricted to cases where blades of rotor 1 (located upstream) are vibrating. In all cases the axial Mach number and the boss ratio are fixed to $M_a = 0.6$ and $h = 0.7$ respectively. Further three cases of blade row configurations shown in Table 2 are dealt with. Note that the relative flow velocity for the rotor blades is supersonic along the whole span for $|\Omega_1| = 3.0$ or $|\Omega_2| = 3.0$, and subsonic along the whole span for $|\Omega_1| = 1.0$ or $|\Omega_2| = 1.0$.

In general it is not easy to obtain precise elastic properties of twisted blades. The main purpose of the present paper is to investigate the effect of the multi-blade-row coupling on the cascade flutter. Therefore

to simplify the problem, let the elastic properties be approximated by those of a uniform flat plate. The bending and torsional mode shape functions of the flat plate are given by

$$\begin{aligned} Z_k(r) &= [(\sin\Gamma_k - \sinh\Gamma_k)(\sinh\{\Gamma_k R(r)\} \\ &\quad - \sin\{\Gamma_k R(r)\}) \\ &\quad +(\cos\Gamma_k + \cosh\Gamma_k)(\cosh\{\Gamma_k R(r)\} \\ &\quad - \cos\{\Gamma_k R(r)\})] \\ &\quad /(\sin\Gamma_k \sinh\Gamma_k), \qquad (46) \\ \Phi_k(r) &= \sqrt{2}\sin\left(\frac{2k-1}{2}\pi R(r)\right), \qquad (47) \end{aligned}$$

where

$$\begin{aligned} R(r) &= \frac{r-h}{1-h}, \quad \Gamma_1 = 0.597\pi, \ \Gamma_2 = 1.49\pi, \\ &\quad \Gamma_k = \frac{2k-1}{2}\pi \ (k \geq 3) \qquad (48) \end{aligned}$$

The shape functions are normalized as

$$\begin{aligned} \frac{1}{1-h}\int_h^1 Z_k(r)Z_j(r)dr &= \delta_{kj}, \\ \frac{1}{1-h}\int_h^1 \Phi_k(r)\Phi_j(r)dr &= \delta_{kj}. \qquad (49) \end{aligned}$$

Further the elastic properties of blades are assumed uniform along the span. In solving the flutter equation (31), vibration modes of the first and second bending orders with the natural frequencies ω_{B1} and ω_{B2} and the first and second torsion orders with the natural frequencies ω_{T1} and ω_{T2} are taken into account. The specified values are as follows; the mass ratio $\mu_{ba} = 120$, the normalized distance between the center of gravity and the elastic axis $x_{eg} = 0.141$, the normalized radius of gyration $r_e = \sqrt{0.6}$, the elastic axis position $z_e/C_a = -0.075$, and the natural frequency ratios $\bar{\omega}_{T1} = \omega_{T1}/\omega_{B1} = 6.0$, $\bar{\omega}_{B2} = \omega_{B2}/\omega_{B1} = 6.3$, $\bar{\omega}_{T2} = \omega_{T2}/\omega_{B1} = 18.0$.

Case sub-sub

Figures 3 and 4 show the flutter reduced frequency $2\lambda_F = \omega_F C_{a1}$ and the dimensionless flutter frequency ω_F/ω_{B1} as functions of the interblade phase parameter σ and the distance between the blade rows G. Here $C_a = (C_{a1} + C_{a2})/2$, and "Decoupled" implies the isolated blade row, i.e., the case of absence of rotor 2. In Figure 3 cut-off boundaries defined by equation (18) are also indicated.

In general cruicial change in the flutter frequency occurs through the cut-off boundaries of the fundamental primary duct mode (0,0; 0). Further it is clear that the effect of blade row coupling, i.e., the deviation from the decoupled case is very small in the range of σ where the fundamental primary duct mode (0,0;0) is cut-off, but it is large in the range of σ where the fundamental primary duct mode (0,0;0) is cut-on.

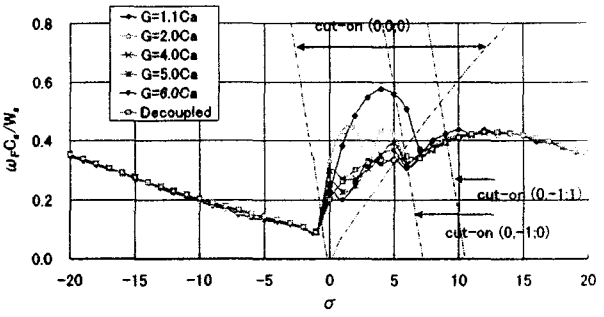

Figure 3: Flutter reduced frequency $\omega_F C_{a1} = 2\lambda_F$ dependent on the interblade phase angle and the blade row gap. Case sub-sub.

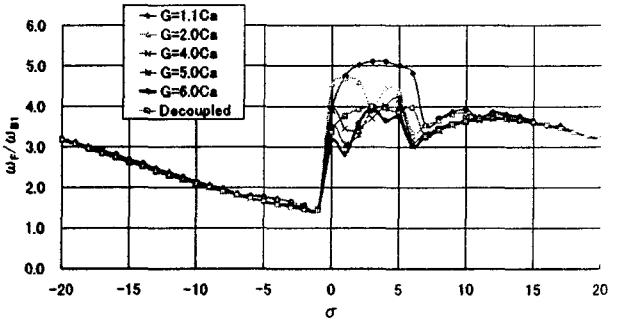

Figure 4: Dimensionless flutter frequency ω_F/ω_{B1} dependent on the interblade phase angle and the blade row gap. Case sub-sub.

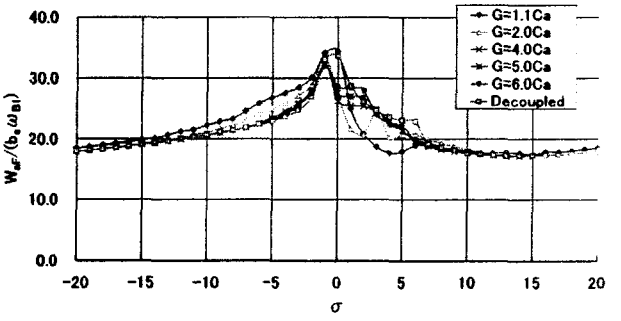

Figure 5: Reduced flutter velocity $W_{aF}/(b_{a1}\omega_{B1})$ dependent on the interblade phase angle and the blade row gap. Case sub-sub.

Table 2: Specified conditions.

Case	N_{B1}	Ω_1	C_{a1}	N_{B2}	Ω_2	C_{a2}
sub-sub	40	1.0	0.1	40	-1.0	0.1
sub-sup	40	1.0	0.1	30	-3.0	0.0633
sup-sub	30	3.0	0.0633	40	-1.0	0.1

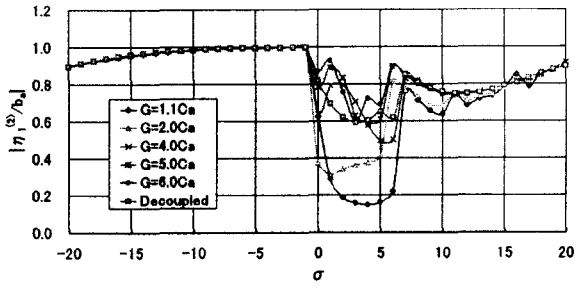

Figure 6: The first bending mode amplitude $|\eta_1/b_{a1}|$ at the flutter condition dependent on the interblade phase angle and the blade row gap. Case sub-sub.

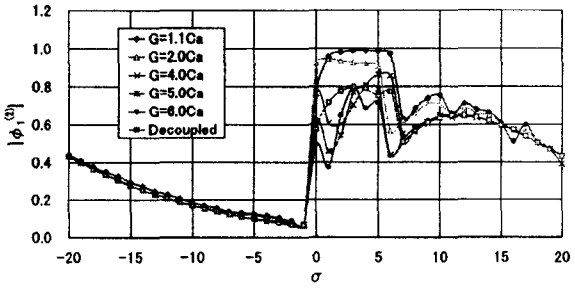

Figure 7: The first torsion mode amplitude $|\phi_1|$ at the flutter condition dependent on the interblade phase angle and the blade row gap. Case sub-sub.

In the cases of small blade row gaps ($G = 1.1C_a$ and $G = 2.0C_a$), the blade row coupling effect is very large and enhances the flutter frequency in the cut-on region of (0,0;0) duct mode, and further not very small just outside the cut-on region of (0,0;0) duct mode. This indicates that the cut-off duct modes also play some role in aeroacoustic interaction between blade rows in the nearfield, where cut-off duct modes do not fully disappear. It is also clear that the blade row coupling effect diminishes as the blade row gap increases in the range of σ where the fundamental primary duct mode (0,0;0) is cut-off. On the other hand in the cut-on region of (0,0;0) duct mode the coupling effect never diminishes by increase of the blade row gap.

Figure 5 shows the reduced flutter velocity $W_{aF}/(b_a\omega_{B1})$. Large effect of blade row coupling is again observed in the range of σ where (0,0;0) duct mode is cut-on. It should be noted also, that in the cases of small blade row gaps ($G = 1.1C_a$ and $G = 2.0C_a$), deviation from the case of the isolated blade row is quite large in the cut-on region of (0,0:0) duct mode , and still significant in the cut-off region of (0,0;0) duct mode. In those cases it can be stated that the effect of blade row coupling decreases the flutter velocity in the cut-on region of the fundamental primary duct mode (0,0;0), but increases the flutter velocity outside the region.

Figures 6 and 7 show absolute values of the modal amplitudes of blade displacement at the flutter condition. First of all drastic change in the flutter mode occurs across the cut-off boundaries of the primary duct mode (0, 0; 0) irrespective of the blade row coupling conditions. In the range of σ where the fundamental primary duct mode (0,0;0) is cut-off, the first bending mode η_1/b_a is predominant at the side of negative σ, while the first bending mode η_1/b_a is still larger but the dominance is smaller at the side of positive σ. On the other hand in the range of σ where (0,0;0) duct mode is cut-on, the first torsion mode ϕ_1 is rather dominant in the case of the isolated blade row and overwhelmingly dominant in the cases of small blade row gaps ($G = 1.1C_a$ and $G = 2.0C_a$). In the cases of longer blade row distances ($G = 4.0C_a$, $5.0C_a$, $6.0C_a$), however, the dominance changes from the first bending mode to the first torsion mode with increase of σ.

Case sub-sup

Figures 8 - 12 show the results of the case sub-sup, where the subsonic rotor 1 of oscillating blades in-

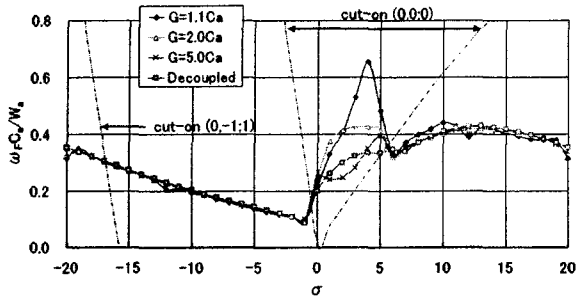

Figure 8: Flutter reduced frequency $\omega_F C_{a1} = 2\lambda_F$ dependent on the interblade phase angle and the blade row gap. Case sub-sup.

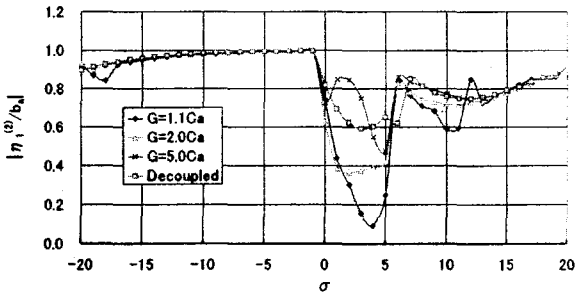

Figure 11: The first bending mode amplitude $|\eta_1/b_{a1}|$ at the flutter condition dependent on the interblade phase angle and the blade row gap. Case sub-sup.

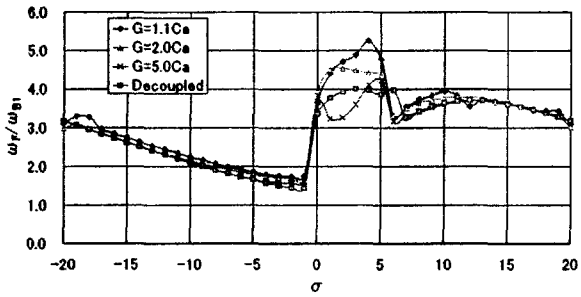

Figure 9: Dimensionless flutter frequency ω_F/ω_{B1} dependent on the interblade phase angle and the blade row gap. Case sub-sup.

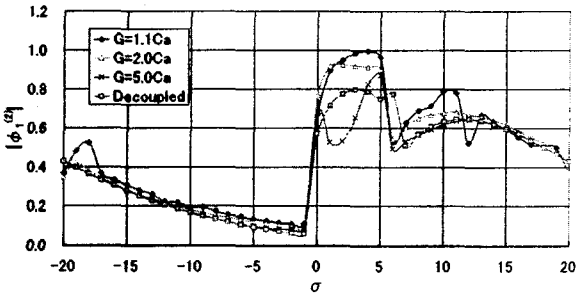

Figure 12: The first torsion mode amplitude $|\phi_1|$ at the flutter condition dependent on the interblade phase angle and the blade row gap. Case sub-sub.

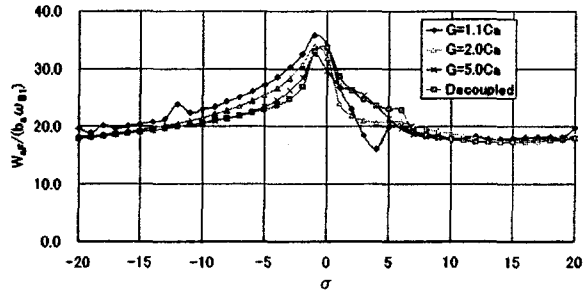

Figure 10: Reduced flutter velocity $W_{aF}/(b_{a1}\omega_{B1})$ dependent on the interblade phase angle and the blade row gap. Case sub-sup.

teracts with the supersonic rotor 2 of non-oscillating blades. The trend of the blade row coupling effects is essentially same as in the case of sub-sub. It is worth mentioning, however, that the non-small effect of the blade row coupling in the cut-off region of the fundamental primary duct mode (0,0;0), in particular, on the flutter velocity, is more clearly observed than in the case of sub-sub (Figure 10).

Case sup-sub

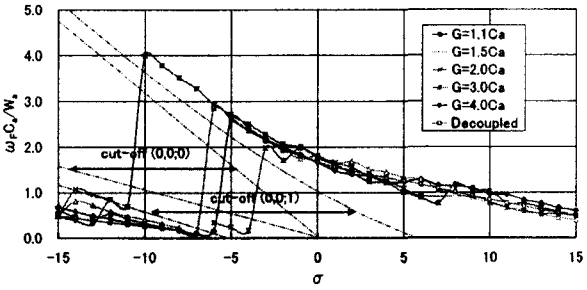

Figure 13: Flutter reduced frequency $\omega_F C_{a1} = 2\lambda_F$ dependent on the interblade phase angle and the blade row gap. Case sup-sub.

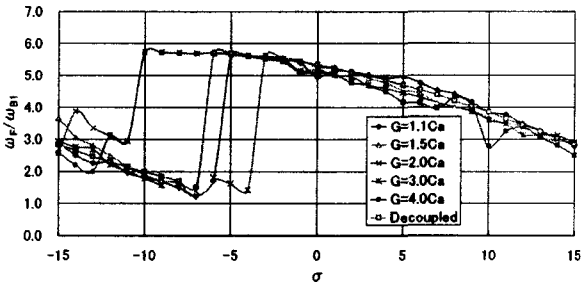

Figure 14: Dimensionless flutter frequency ω_F/ω_{B1} dependent on the interblade phase angle and the blade row gap. Case sup-sub.

Figures 13 - 17 show the results of case sup-sub, where the supersonic rotor 1 of oscillating blades interacts with the subsonic rotor 2 of non-oscillating blades. First of all it should be mentioned that the flutter characteristics of the supersonic rotor is quite different from those of the subsonic rotors (cases sub-sub and sub-sup). With respect to this matter, it should be noted that the range of σ where the fundamental primary duct mode (0,0;0) is cut-off is very narrow in the case of supersonic blade rows.

As Figure 13 shows no flutter occurs in the range of σ where the fundamental primary duct mode $(0, 0; 0)$ is cut-off. Thus in the range of negative σ, the flutter

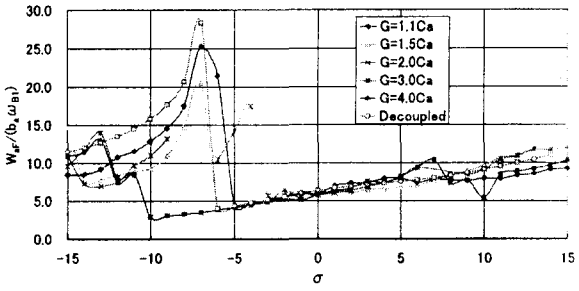

Figure 15: Reduced flutter velocity $W_{aF}/(b_{a1}\omega_{B1})$ dependent on the interblade phase angle and the blade row gap. Case sup-sub.

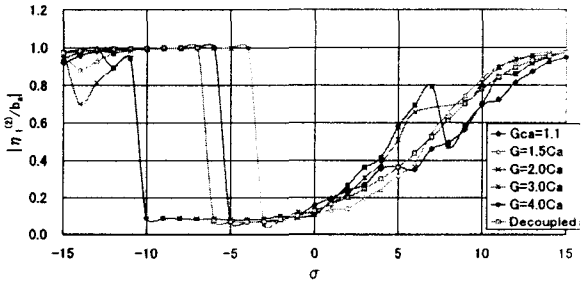

Figure 16: The first bending mode amplitude $|\eta_1/b_{a1}|$ at the flutter condition dependent on the interblade phase angle and the blade row gap. Case sup-sub.

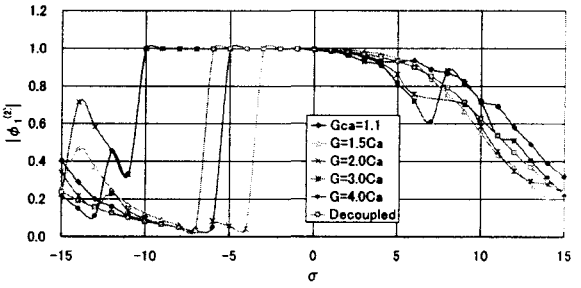

Figure 17: The first torsion mode amplitude $|\phi_1|$ at the flutter condition dependent on the interblade phase angle and the blade row gap. Case sup-sub.

reduced frequency $\omega_F C_{a1}$ jumps from the lower cut-on side $\omega_F < \omega^-_{(0,0,0)}$ to the upper cut-on side $\omega_F > \omega^+_{(0,0,0)}$ with a small change in σ. Note that σ only takes integral numbers, and the jump occurs by just one step change in σ. More close observation reveals that the flutter is unlikely to occur also in the range of σ where the second primary duct mode $(0, 0; 1)$ is cut-off.

A jumping up of the reduced flutter frequency is accompanied by jumping down of the reduced flutter velocity (Figure 15), and change of dominance of the flutter mode from the first bending mode to the first torsion mode (Figures 16 and 17).

The effect of the blade row coupling is generally large and it is worth emphasizing that the interblade phase angle across which the flutter point jumps is highly dependent on the blade row gap.

Finally it should also be pointed out that the reduced flutter velocity of the supersonic rotor (case sup-sub) is generally lower than that of the subsonic rotor (cases sub-sub and sub-sup).

Conclusions

(1) The effect of the neighboring blade row on the flutter characteristics is closely related to the state (cut-on, cut-off, near resonance) of primary duct modes.
(2) In the case of vibrating subsonic blade row the effect of blade row coupling is large in the range of the interblade phase angle where the fundamental primary duct mode is cut-on.
(3) In the case of vibrating subsonic blade row the closely placed neighbor blade row gives non-small influence on the reduced flutter velocity even in the range outside of the cut-on primary duct mode of the lowest order, and the influence is higher in the case of the supersonic neighbor blade row.
(4) In the case of vibrating supersonic blade row no flutter occurs in the range where the fundamental primary duct mode is cut-off, and the flutter point jumps across the cut-off region.
(5) The interblade phase angle across which the flutter point jumps is highly dependent on the blade row gap.

References

[1] Tanida,Y., "Effect of Blade Row Interference on Cascade Flutter," *Transactions of Japan Society for Aeronautical and Space Sciences*, **Vol. 9, No. 15**, 1966, pp.100-108.

[2] Kobayashi, H., Tanaka, H. and Maruta, H., "Effect of Rotor-Stator Interaction on Cascade Flutter, 1st Report: Experimantal Study on Pure Bending Mode of Compressor Cascade," *Transactions of Japan Society for Mechanical Engineers*, **Vol. 40, No. 334**, 1974, pp.1615-1626.

[3] Kobayashi, H., Tanaka, H. and Hanamura, Y., "Effect of Rotor-Stator Interaction on Cascade Flutter, 2nd Report: Theoretical Study on Pure Bending Mode," *Transactions of Japan Society for Mechanical Engineers*, **Vol. 41, No. 346**, 1975, pp.1770-1780.

[4] Butenko, K.K. and Osipov, A.A., "Unsteady Subsonic Flow Past Two Relatively Moving Flat Cascades of Thin Weakly Loaded Oscillating Blades," *Fluid Dynamics*, **Vol. 22**, 0015-4628/88/2304-0620, Plenum Publishing Corporation, New York, 1989, pp.620-625.

[5] Hall, K.C. and Silkowski, P.D., "The Influence of Neighboring Blade Rows on the Unsteady Aerodynamic Response of Cascades", *ASME J. of Turbomachinery*, **Vol. 119**, 1997, pp.85–93.

[6] Hall, K.C., Ekici, K. and Voytovych, D.M., "Multistage Coupling for Unsteady Flows in Turbomachinery", *Proceedings of 10th International Symposium on Unsteady Aerodynamics, Aeroacoustics and Aeroelasticity of Turbomachines*, held at Duke University in September 2003, to be published.

[7] Namba, M., Yamasaki, N. and Nishimura, S., "Unsteady Aerodynamic Force on Oscillating Blades of Counter-Rotating Annular Cascades," Proceedings of 9th International Symposium on Unsteady Aerodynamics, Aeroacoustics and Aeroelasticity of Turbomachines, Presses Universitaires de Grenoble, 2001.

[8] Namba, M., "Unsteady Aerodynamic Response of Oscillating Supersonic Annular Cascades in Counter Rotation", *AIAA Meeting Papers on Disk*, Vol.6, No.3, 37th AIAA/ASME/SAE Joint Propulsion Conference, AIAA Paper No. 2001-3741, 2001.

[9] Namba, M. and Ishikawa, A., "Three-Dimensional Aerodynamic Characteristics of Oscillating Supersonic and Transonic Annular Cascades," *ASME J. of Engineering for Power*, **Vol. 105**, 1983, pp.138-146.

[10] Namba, M., "Three-Dimensional Flows," *AGARD Manual on Aeroelasticity in Axial Flow Turbomachines, Vol. 1, Unsteady Turbomachinery Aerodynamics*, **AGARD-AG-298**. M.F. Platzer and F.O. Carta, eds., Neuilly sur Seine, France, 1987.

[11] Namba, M. and Nanba, K., "Unsteady Aerodynamic Work on Oscillating Annular Cascades in Counter Rotation: Combination of Supersonic and Subsonic Cascades", *Proceedings of 10th International Symposium on Unsteady Aerodynamics, Aeroacoustics and Aeroelasticity of Turbomachines*, held at Duke University in September 2003, to be published.

Appendix

Philosophy to Determine Blade Loading

The disturbance flow field can be expressed as summation of disturbances induced by unsteady blade loadings of both rotors. In the case of vibration of rotor 1 blades expressed by equation (2), the disturbance velocity $\boldsymbol{q}$ is expressed in the form

$$\begin{aligned}\boldsymbol{q} &= \sum_{\nu=-\infty}^{\infty} e^{i\omega_{1\nu}t}\int_h^1\int_{-C_{a1}/2}^{C_{a1}/2}\Delta p_{1-1,(\nu)}(\rho,\zeta)\\ &\quad\times\boldsymbol{K}_q(r,\eta_1,z_1-\zeta\,|\,\rho;\,N_{B1},\Omega_1,\omega_{1\nu},\sigma_{1\nu})d\zeta d\rho\\ &+\sum_{\mu=-\infty}^{\infty} e^{i\omega_{2\mu}t}\int_h^1\int_{-C_{a2}/2}^{C_{a2}/2}\Delta p_{2-1,(\mu)}(\rho,\zeta)\\ &\quad\times\boldsymbol{K}_q(r,\eta_2,z_2-\zeta\,|\,\rho;\,N_{B2},\Omega_2,\omega_{2\mu},\sigma_{2\mu})d\zeta d\rho,\end{aligned}\tag{A.1}$$

where η_1 and η_2 are helical coordinates defined by

$$\eta_1=\theta_1-\Omega_1 z_1,\quad \eta_2=\theta_2-\Omega_2 z_2.\tag{A.2}$$

Note that the m-th blade of rotor j is placed on the surface $\eta_j=2\pi m/N_{Bj}$.

The kernel function $\boldsymbol{K}_q$ denotes the disturbance velocity induced by an annular row of pressure dipoles of fluctuating strength with unit amplitude, and it is exactly same as that for a single cascade model[9, 10]. It involves not only acoustic disturbances but also vortical disturbances convected downstream from the dipole points. This is further decomposed into circumferential modes in the form

$$\begin{aligned}&\boldsymbol{K}_q(r,\eta_j,z_j-\zeta\,|\,\rho;\,N_{Bj},\Omega_j,\omega_{j\mu},\sigma_{j\mu})\\ &=\sum_{\nu=-\infty}^{\infty} e^{i(\nu N_{Bj}+\sigma_{j\mu})\eta_j}\\ &\quad\times\boldsymbol{K}_q^{(\nu)}(r,z_j-\zeta\,|\,\rho;\,N_{Bj},\Omega_j,\omega_{j\mu},\sigma_{j\mu})\end{aligned}\tag{A.3}$$

Here $n=\nu N_{Bj}+\sigma_{j\mu}=\nu N_{Bj}+\mu N_{Bk}+\sigma$ is a circumferential wave number and $R_\ell^{(n)}(r)$ denotes a radial eigenfunction of order ℓ as used in references [9, 10]. We should note that the blade loadings are not prescribed but should be determined so that the disturbance velocity given by equation (A.1) satisfies the flow tangency condition on the blade surfaces of both rotors. The expression (A.1) with the blade loading functions determined in this way automatically includes phenomena of reflection and transmission of disturbances at the rotors.

The flow tangency condition at the blade surfaces can be expressed by

$$[q_{\perp 1}]_{\eta_1=0} = \left(i\omega a_1(r,z_1)+\frac{\partial a_1(r,z_1)}{\partial z_1}\right)e^{i\omega t}\quad:\ -\frac{C_{a1}}{2}\le z_1\le\frac{C_{a1}}{2},\tag{A.4}$$

$$[q_{\perp 2}]_{\eta_2=0} = 0\quad:\ -\frac{C_{a2}}{2}\le z_2\le\frac{C_{a2}}{2},\tag{A.5}$$

where $q_{\perp j}$ denotes the disturbance velocity component normal to rotor j blade surfaces. Equations (A.4) and (A.5) can be rewritten into a set of simultaneous integral equations for the unsteady blade loading functions as follows:

$$\begin{aligned}&\int_h^1\int_{-C_{a1}/2}^{C_{a1}/2}\Delta p_{1-1,(\nu)}(\rho,\zeta)\\ &\times K_{q\perp}(r,0,z_1-\zeta\,|\,\rho;\,N_{B1},\Omega_1,\omega_{1\nu},\sigma_{1\nu})d\zeta d\rho\\ &+\sum_{\mu=-\infty}^{\infty} e^{i(\mu N_{B1}+\sigma_{1\nu})(\Omega_{12}z_1+\Omega_2 G)}\\ &\times\int_h^1\int_{-C_{a2}/2}^{C_{a2}/2}\Delta p_{2-1,(\mu)}(\rho,\zeta)\\ &\times K_{q\perp 1-2}^{(\nu)}(r,z_1-G-\zeta\,|\,\rho;\,N_{B2},\Omega_2,\omega_{2\mu},\sigma_{2\mu})d\zeta d\rho\\ &=\left(i\omega a_1(r,z_1)+\frac{\partial a_1(r,z_1)}{\partial z_1}\right)\delta_{\nu,0}\\ &:\ -\frac{C_{a1}}{2}\le z_1\le\frac{C_{a1}}{2},\end{aligned}\tag{A.6}$$

$$\begin{aligned}&\int_h^1\int_{-C_{a2}/2}^{C_{a2}/2}\Delta p_{2-1,(\nu)}(\rho,\zeta)\\ &\times K_{q\perp}(r,0,z_2-\zeta\,|\,\rho;\,N_{B2},\Omega_2,\omega_{2\nu},\sigma_{2\nu})d\zeta d\rho\\ &+\sum_{\mu=-\infty}^{\infty} e^{-i(\mu N_{B2}+\sigma_{2\nu})(\Omega_{12}z_2+\Omega_1 G)}\\ &\times\int_h^1\int_{-C_{a1}/2}^{C_{a1}/2}\Delta p_{1-1,(\mu)}(\rho,\zeta)\\ &\times K_{q\perp 2-1}^{(\nu)}(r,z_2+G-\zeta\,|\,\rho;\,N_{B1},\Omega_1,\omega_{1\mu},\sigma_{1\mu})d\zeta d\rho\\ &=0\quad:\ -\frac{C_{a2}}{2}\le z_2\le\frac{C_{a2}}{2}.\\ &\nu=0,\pm1,\pm2,\ldots\end{aligned}\tag{A.7}$$

Truncating the infinite series into finite series, one can numerically solve the equations by a standard method.

The mathematical process to derive the kernel functions and their expressions are omitted to save space, but can be referred to references[9, 10].

In the case of blade vibration of rotor 2 with displacement normal to blade surface given by equation (9), similar formulations can be made.

II: Definitions of Parameters in Matrices $\boldsymbol{M}_{kj}$, $\boldsymbol{S}_{kj}$, $\boldsymbol{K}_{kj}$, and $\boldsymbol{A}_{kj}$

Define

$$m(r) = r_T^*\int_{-b(r)}^{b(r)}\rho_b(r,s)ds\tag{A.8}$$

: blade mass per unit span

$$I_e(r) = r_T^{*3}\int_{-b(r)}^{b(r)}\rho_b(r,s)\{s-s_e(r)\}^2 ds\tag{A.9}$$

: moment of inertia per unit span

$\rho_b(r,s)$: blade mass per unit surface area (A.10)

Note that each set of the natural mode shape functions $Z_1,(r), Z_2,(r),\ldots$ and $\Phi_1(r), \Phi_2(r),\ldots$ is orthogonal with weight functions $m(r)$ or $I_e(r)$ as follows:

$$r_T^* \int_h^1 m(r) Z_k(r) Z_j(r) dr = M_j \delta_{kj}, \quad \text{(A.11)}$$

$$r_T^* \int_h^1 I_e(r) \Theta_k(r) \Theta_j(r) dr = I_j \delta_{kj}. \quad \text{(A.12)}$$

Equations (A.11) and (A.12) also define generalized mass M_j and generalized moment of inertia I_j respectively.

$$S_{jk} = r_T^* \int_h^1 S_e(r) Z_j(r) \Theta_k(r) dr, \quad \text{(A.13)}$$

$$S_e(r) = r_T^{*2} \int_{-b(r)}^{b(r)} \rho_b(r,s)\{s - s_e(r)\} ds \quad \text{(A.14)}$$

: Static mass moment per unit span

The modal lift and moment coefficients are defined by

$$\begin{Bmatrix} L_{Bkj} \\ L_{Tkj} \end{Bmatrix} = \frac{1}{\pi(1-h)} \int_h^1 Z_k(r) dr \times \frac{1}{b_a} \int_{-b(r)}^{b(r)} \begin{Bmatrix} \Delta p_{Bj}(r,s) \\ \Delta p_{Tj}(r,s) \end{Bmatrix} ds, \quad \text{(A.15)}$$

$$\begin{Bmatrix} M_{Bkj} \\ M_{Tkj} \end{Bmatrix} = \frac{1}{\pi(1-h)} \int_h^1 \Phi_k(r) dr \times \frac{1}{b_a^2} \int_{-b(r)}^{b(r)} \begin{Bmatrix} \Delta p_{Bj}(r,s) \\ \Delta p_{Tj}(r,s) \end{Bmatrix} \times \{s - s_e(r)\} ds \quad \text{(A.16)}$$

Further define

$$M_b = r_T^* \int_h^1 m(r) dr \quad \text{(A.17)}$$

: total mass of the blade,

$$I_{be} = r_T^* \int_h^1 I_e(r) dr \quad \text{(A.18)}$$

: total moment of inertia of the blade,

$$S_{be} = r_T^* \int_h^1 S_e(r) dr \quad \text{(A.19)}$$

: total static mass moment of the blade,

$$M_{air} = r_T^{*3} \pi \rho b_a^2 (1-h) \quad \text{(A.20)}$$

: mass of air in a cylindrical volume of radius $r_T^* b_a$ and height $r_T^*(1-h)$ (A.21)

$$\mu_{ba} = M_b / M_{air} \text{ : mass ratio,} \quad \text{(A.22)}$$

$$x_{eg} = S_{be} / (M_b r_T^* b_a) \quad \text{(A.23)}$$

: averaged dimensionless distance between c.g. (the center of gravity) and e.a. (the elastic axis) normalized by $r_T^* b_a$, (A.24)

$$r_e = \sqrt{I_{be} / (M_b r_T^{*2} b_a^2)} \text{ : averaged dimensionless radius of gyration normalized by } r_T^* b_a \text{ .} \quad \text{(A.25)}$$

Finally nondimensional generalized modal mass $\bar{M}_i$, modal moment of inertia $\bar{I}_k$ and modal static mass moment $\bar{S}_{ik}$ are defined by

$$\bar{M}_k = M_k / M_b, \quad \text{(A.26)}$$

$$\bar{I}_k = I_k / I_{be}, \quad \text{(A.27)}$$

$$\bar{S}_{jk} = S_{jk} / S_{be}. \quad \text{(A.28)}$$

Note that we have

$$\frac{M_k}{M_{air}} = \frac{M_b}{M_{air}} \frac{M_k}{M_b} = \mu_{ba} \bar{M}_k,$$

$$\frac{S_{kj}}{M_{air}} = \frac{M_b}{M_{air}} \frac{S_{kj}}{S_{be}} \frac{S_{be}}{M_b} = \mu_{ba} \bar{S}_{kj} r_T^* b_a x_{eg},$$

$$\frac{I_k}{M_{air}} = \frac{M_b}{M_{air}} \frac{I_{be}}{M_b} \frac{I_k}{I_{be}} = \mu_{ba} r_T^{*2} b_a^2 r_e^2 \bar{I}_k.$$